Horvath, L.; Koncz, P.; Moring, A.; Nagy, Z.; Pintér, K.; Weidinger, T. 2018.
An attempt to partition stomatal and non-stomatal ozone deposition parts on a short grassland.

This is a post-peer-review, pre-copyedit version of an article published in *Boundary-Layer Meteorology*, 167 (2). 303-326. The final authenticated version is available online at: https://doi.org/10.1007/s10546-017-0310-x.

An attempt to partition stomatal and non-stomatal ozone deposition parts on a short grassland

L. Horváth[1,2] • P. Koncz[2] • A. Móring[1,3] • Z. Nagy [2,4] • K. Pintér[2,4] • T. Weidinger[5]

Abstract To evaluate the damaging effect of tropospheric ozone on vegetation, it is important to evaluate the stomatal uptake of ozone. Although stomatal flux is a dominant pathway of ozone deposition onto vegetated surfaces, non-stomatal uptake mechanisms as soil deposition, especially when $LAI < 4$, and cuticular deposition are also vital parts. In this study, we partitioned canopy conductance into stomatal and non-stomatal parts. To calculate the stomatal conductance of water vapour for sparse vegetation, firstly, we partitioned the latent heat flux into transpiration and evaporation parts using the Shuttleworth-Wallace (SW) model. Then we derived the stomatal conductance of ozone by the Penman-Monteith (PM) theory based on the similarity to water vapour conductance. The non-stomatal conductance was calculated by subtracting the stomatal conductance from canopy conductance derived from direct flux measurement data. Our results show that for short vegetation ($LAI = 0.25$) dry deposition of ozone was dominated by non-stomatal flux, exceeding stomatal flux even in daytime, while at night stomatal uptake of ozone was negligibly small. In the case of vegetation with $LAI \approx 1$, the daytime stomatal and non-stomatal fluxes were of the same order of magnitude. These results underline that non-stomatal processes have to be considered even in the case of well-developed vegetation where cuticular uptake is comparable in magnitude with stomatal uptake, and especially in the case of vegetated surfaces with $LAI < 4$ where soil uptake takes part in ozone deposition as well.

Keywords Deposition • Eddy covariance • Non-stomatal conductance • Ozone flux • Stomatal conductance

✉ L. Horváth
horvath.laszlo.dr@gmail.com; horvath.l@met.hu

[1]Hungarian Meteorological Service, Gilice tér 39, Budapest, 1181, Hungary

[2]MTA-SZIE Plant Ecology Research Group, Szent István University, Páter Károly utca 1, Gödöllő, 2100, Hungary

[3]Centre for Ecology and Hydrology, Penicuik, EH16 0QB, United Kingdom and University of Edinburgh, Edinburgh, EH9 3JN, United Kingdom

[4]Institute of Botany and Plant Physiology, Szent István University, Páter Károly utca 1, Gödöllő, 2100, Hungary

[5]Department of Meteorology, Eötvös Loránd University, Pázmány Péter sétány 1/A, 1117 Budapest, Hungary

List of symbols

Symbol	Name	Unit
AGB	above ground green biomass	g m^{-2}
b_1; b_3	empirical constants for estimation of r_{ss}	s m^{-1}
b_2	empirical constant for estimation of r_{ss}	--
c	concentration of ozone at the reference height (= 4 m)	nmol m^{-3}
$\mathrm{C_c}$; $\mathrm{C_s}$	canopy and surface resistance coefficients in the SW model	--
c_p	specific heat capacity of moist air at constant pressure (= 1,013)	J kg^{-1} K^{-1}
c_{pv}	specific heat capacity of water vapour at constant pressure (= 1,850)	J kg^{-1} K^{-1}
c_w	specific heat capacity of water (= 4,220)	J kg^{-1} K^{-1}
d	displacement height	m
D	vapour pressure deficit in the air	Pa
D_{O_3}/D_w	molecular diffusivity ratio of ozone to water (= 0.608)	--
E	ecosystem evapotranspiration (water vapour flux)	kg m^{-2} s^{-1}
E_e	evaporation of soil water and other wet surfaces	kg m^{-2} s^{-1}
E_t	stomatal transpiration	kg m^{-2} s^{-1}
e	water vapour pressure	Pa
e_s	saturated water vapour pressure	Pa
F	ozone flux	nmol m^{-2} s^{-1}
G	heat flux into the soil	W m^{-2}
h	vegetation height	m
H	sensible heat flux	W m^{-2}
k	Kármán constant (= 0.4)	--
L	Obukhov length	--
LAI	leaf area index (green fraction)	m^2 m^{-2}
LW	leaf surface wetness	%
n	eddy diffusivity decay constant (= 2.5)	--
p	air pressure	Pa
PM_c	canopy transpiration in the SW model	W m^{-2}
PM_s	soil evaporation in the SW model	W m^{-2}
r	total resistance to ozone dry deposition	s m^{-1}
r_a	aerodynamic resistance	s m^{-1}
r_b	boundary layer resistance	s m^{-1}
r_c	canopy resistance	s m^{-1}
r_{st}	bulk stomatal resistance including mesophyll resistance r_{mes}	s m^{-1}
r_{nst}	non-stomatal resistance	s m^{-1}
r_{aa}	resistance of canopy height to reference height in the SW model	s m^{-1}
r_{ac}	bulk boundary layer resistance of the vegetative elements in the canopy in the SW model	s m^{-1}
r_{as}	resistance of soil surface to canopy height in the SW model	s m^{-1}
r_{bv}	mean boundary layer resistance per unit area of vegetation in the SW model (= 25)	s m^{-1}
r_{mst}	mean stomatal resistance in the SW model (= 400)	s m^{-1}
r_{sc}	canopy stomatal resistance in the SW model	s m^{-1}
r_{ss}	soil surface resistance in the SW model	s m^{-1}
RH	relative humidity	%
R	available energy input above the canopy	W m^{-2}

R_g	global radiation	W m^{-2}
R_n	net radiation	W m^{-2}
R_{ns}	net radiation fluxes to soil	W m^{-2}
R_s	available energy input above the soil surface	W m^{-2}
R_w	specific gas constant for water vapour (= 461.5)	J kg^{-1} K^{-1}
Sc/Pr	ratio of the Schmidt to the Prandtl number (= 1.486)	--
t_a; t_s	air; soil temperature	°C
t	time	s
T	air temperature	K
u	wind velocity at the reference height (x)	m s^{-1}
u_*	friction velocity	m s^{-1}
U	electric voltage	mV
v_d	dry deposition velocity of ozone	m s^{-1}
z	reference height of measurements above canopy (= 4)	m
z_0	roughness length	m
β	Bowen-ratio (= $H/\lambda E$)	--
γ	psychrometric constant [= $c_p\, p/(\lambda\, \varepsilon)$]	Pa K^{-1}
δ	water vapour density saturation deficit	kg m^{-3}
Δ	slope of the saturation vapour pressure [= $e_s\, \lambda/(R_w\, T^2)$]	Pa K^{-1}
ε	ratio of mean molar mass of water to dry air (= 0.6215)	--
θ	soil water content	volume %
θ_s	saturated soil water content (= 28 at measuring site)	volume %
κ_c	canopy conductance	m s^{-1}
κ_{nst}	non-stomatal conductance	m s^{-1}
κ_{st}	stomatal conductance including mesophyll conductance	m s^{-1}
λ	latent heat of vaporization [λ_0 = 2,500,800 at 0 °C, $\lambda = \lambda_0 + (c_{pv} - c_w) t_a$]	J kg^{-1}
λE	latent heat flux	W m^{-2}
λE_e	latent heat flux from the soil surface	W m^{-2}
λE_t	latent heat flux from the canopy	W m^{-2}
ρ	density of moist air (calculated from *RH*, *T*, *p*)	kg m^{-3}
ρ_v	density of water vapour	kg m^{-3}
ρ_{vs}	density of saturated water vapour	kg m^{-3}
ρ_a; ρ_s; ρ_c	parameters in calculation of C_c and C_s	Pa s K^{-1} m^{-1}
τ	momentum flux	kg m^{-1}s^{-2}
Φ	relative ozone flux	mV m s^{-1}
ζ	dimensionless height (= z/L)	--

1 Introduction

The harmful effects of ozone on plants are well known (Amann et al. 2011, Colette et al. 2012). Ozone molecules enter via the stomata; therefore, the risk of ozone damage can be quantified by stomatal uptake, rather than by simple exposure-based indices like SUM06, W126 and AOT40 (Emberson et al. 2000, Massman 2004, Musselman et al. 2006, Mills et al. 2011).

Ozone flux measurements generally allow the aerodynamic, boundary layer and canopy resistances (r_a, r_b, and r_c, respectively) to be separated on the basis of resistance analogy models. Canopy resistance includes both stomatal and mesophyll components (in this paper the sum of these two parts is referred to as stomatal) and so-called non-stomatal resistance, consisting of the deposition to leaf cuticle, the ground, litter and other parts of the plant, as well as near-surface chemistry.

Several examples of methods can be found in the literature to calculate the stomatal conductance of ozone. For example, Rummel et al. (2007) applied a modified Jarvis-type model (Jarvis 1976) derived for water vapour flux, using maximum stomatal conductivity ($\kappa_{st,max}$), *LAI* and functions for specific humidity deficit, t_a, and short wave radiation. According to the compilation of Kelliher et al. (1995), the $\kappa_{st,max}$ is site- and vegetation-specific and ranges between 6-12 mm s^{-1} at optimum meteorological conditions, which makes it difficult to generalise the method. Another example was published by Granz et al. (1995). They also used the similarity between the stomatal conductance of ozone and water vapour, deriving a simple empirical equation for κ_{st} expressed as a function of photosynthetically active radiation. Massman (2004) described a simple empirical method for a vineyard site, using solar radiation and *LAI* as inputs. The disadvantage of this calculation is that the model is site-specific.

The canopy model by Wang and Leuning (1998) used a simple model to partition the available energy and calculate the stomatal conductance for CO_2. The parameterisation of stomatal conductance involves, among others, the net photosynthetic and carboxylation rates, which are not widely available parameters. In this approach, a single-layer canopy model calculates the fluxes of sensible heat, latent heat, and CO_2, separately for sunlit and shaded leaves. Compared to a multi-layer model (assuming ozone deposition takes place separately on different parts of the canopy), the CO_2, latent and sensible heat fluxes predicted usually agreed with a less than 5% difference over a typical range of leaf area index values for a wheat crop grown in a temperate climate.

Lamaud et al. (2002) estimated the stomatal conductance for ozone using the mechanism mentioned above, based on the similarity to the water vapour flux, for a pine forest canopy in dry and wet conditions. Ozone fluxes were measured using the eddy covariance (EC) technique above and within the canopy. They demonstrated that the ozone uptake by the understory is a significant proportion of the entire ozone deposition onto the whole pine stand. According to their results, the understory contributes more to the overall ozone flux than to the other measured scalar fluxes (sensible heat and water vapour). Also, during the day, in dry conditions, the canopy stomatal conductance is the major parameter controlling ozone deposition. Furthermore, in winter, the influence of dynamic processes persists during daytime. It was also found that surface wetness associated with dew significantly enhanced ozone deposition during the night as well as in the morning.

Lamaud et al. (2009) partitioned ozone deposition over a developed maize crop into stomatal and non-stomatal uptakes using eddy covariance flux measurements and modelling. Data were analysed using a big-leaf model, which was developed based on the current knowledge of ozone deposition. In-canopy aerodynamic resistance, intrinsic ground resistance and cuticular resistance were determined from the relationship between experimental non-stomatal conductance and friction velocity in dry conditions. Non-stomatal conductance was determined as the difference between canopy conductance and stomatal conductance, where the latter was estimated by a method that combines the PM (Penman-Monteith) approach with the use of the similarity to carbon dioxide flux. They showed that the relative contributions of stomatal and non-stomatal uptakes varied strongly with the physiological activity of the maize and the meteorological conditions.

Gerosa et al. (2007) compared different algorithms for stomatal ozone flux determination from micrometeorological measurements using the similarity between ozone stomatal fluxes and water vapour stomatal fluxes. A series of observations, made during the growing season over an onion field, were used to show the equivalence of two algorithms from the literature to derive the stomatal fluxes of ozone. One of these algorithms uses the PM approach, where the water vapour pressure deficit is calculated using air temperature. The second calculates, using another formulation, the water vapour deficit based on leaf temperature. As they argued, the two approaches led to the same results if applied properly, both theoretically and numerically.

Gerosa et al. (2012) modelled stomatal conductance to estimate the evapotranspiration of natural and agricultural ecosystems on an hourly basis. In these cases, the big-leaf approach, together with the resistance analogy that simulates the gas-exchange between vegetation and atmosphere, is a simple but valid example of a process-based model which includes stomatal conductance behaviour, as well as a basic representation of the canopy features.

Coyle et al. (2009) calculated the non-stomatal resistance of ozone as the residual of the difference of canopy resistance and stomatal resistance over a potato field. The stomatal part was estimated using the similarity between the fluxes of water vapour and ozone. In this study, it was assumed that transpiration is the only source of water vapour from the surface.

In most of these approximations, it is assumed that water vapour flux consists only of the water loss from stomata through transpiration (E_t), which is true for well-developed vegetation, especially for forests, where the leaf area index is $LAI > 4$ and the surface is dry. In the case of low vegetation (e.g. grass surfaces), however, water vapour flux can also be derived from evaporation (E_e) from other wet surfaces, especially from the ground. Over bare soil there is no transpiration; and in parallel with increasing *LAI*, the share of transpiration in the total evapotranspiration increases as well. At $LAI = 4$ (a practically closed canopy) the share of transpiration is still 91-94% (Shuttleworth and Wallace 1985), hence evaporation is nearly negligible. However, below $LAI = 4$ water vapour flux cannot be used to estimate the stomatal conductance of ozone, therefore transpiration and evaporation rates have to be separated.

In the ÉCLAIRE EU 7th Framework Program project (Sutton et al. 2013) we monitored the ozone flux by the eddy covariance method above short vegetation (grassland) between August 2012 and January 2014. As a result of the mean leaf area index ($LAI_{mean} = 0.5$) in the observation period, when calculating the different deposition parts, in addition to the transpiration, we also had to take into account the potential effect of evaporation.

The aim of the current study is to derive stomatal conductance (κ_{st}) based on the partitioning of water vapour flux. This also lets us calculate the stomatal flux of ozone, which is an important factor in the estimation of the damage caused by the direct uptake of ozone. In addition, once κ_{st} is obtained, non-stomatal conductance (κ_{nst}) can also be derived as the residual term: $\kappa_{nst} = \kappa_c - \kappa_{st}$. The κ_{nst} values estimated in this way can serve as a basis for future work, for finding empirical equations that express κ_{nst}. Hence the bulk canopy conductance and dry deposition velocity can be calculated as the function of meteorological variables (including calculated $r_a + r_b$). In this way, we were able to obtain the total ozone fluxes using only data from a slow ozone monitor instead of eddy covariance flux measurement. Such an approach would be useful during gap-filling when eddy covariance ozone flux measurements are not available or when assumptions for eddy covariance (EC) are not satisfied.

Therefore, firstly, we calculated the dry eddy flux of ozone and the canopy resistance. Secondly, we partitioned the latent heat fluxes into fluxes from the canopy and from the surface by the SW (Shuttleworth-Wallace) model (Shuttleworth and Wallace 1985, Hu et al.

2009) resulting in evaporation and transpiration, respectively. Thirdly, we used the transpiration part to calculate stomatal conductance using the inverted PM equation as suggested by Lamaud et al. (2002). Finally, we partitioned stomatal and bulk non-stomatal conductances and we investigated them under different meteorological conditions.

2 Methodology

2.1 Site of Investigations

One of the selected grassland stations of the ÉCLAIRE project is Bugacpuszta on the Hungarian Great Plain (46.69° N, 19.60° E, 113 m a.s.l.). A detailed description of the site was given by Machon et al. (2015). The climate of this semi-natural, semi-arid, sandy grassland is temperate continental, the mean annual temperature is 10.7 °C and the average yearly precipitation is 550 mm. The region has Chernozem-type sandy soil with a high sand (79%) and low clay (13%) content in the upper 10-cm soil layer. The area within 200 m of the measurement plot has never been ploughed. Apart from grazing by a herd of the ancient Grey Cattle breed at an average grazing pressure of 0.5-0.8 stock ha^{-1} in the grazing season (220 days each year) – which has been going on for centuries in dynamic equilibrium with the grass ecosystem (Machon et al. 2010) – the soil has been undisturbed. The plant association is semi-arid sandy grassland (*Cynodonti Festucetum pseudovinae*) dominated by *Festuca pseudovina*, *Carex stenophylla*, and *Cynodon dactylon* (Koncz et al. 2014).

2.2 Measurements

Measurements were conducted between August 2012 and January 2014. The fast response ozone monitor was not operating between the middle of May and the beginning of August 2013 due to a fault. In this study we used the whole (≈ 15 month) dataset for a general picture as well as short (5-12 days) periods to examine the applicability of the coupled SW and PM models to estimate the stomatal conductance of ozone. The list of measured parameters, the methods, and the sampling/logging time are compiled in Table 1.

The ultrasonic anemometer and the inlet of the fast response ozone monitor were arranged at a height of 4 m. The air inlet and the sensor were connected by a 3-m PTFE tube. The air flow during sampling and calibration was 2 L min^{-1}. Sensor disks were provided by the manufacturer as described by Schurath et al. (1991).

INSERT HERE TABLE 1

The HORIBA APOA 350 ozone monitor was calibrated before and after installation (in July 2002 and in January 2004) in the reference laboratory of the Hungarian Meteorological Service by a UV photometric system. During the campaign, we checked the sensitivity and drift of the instrument by gas phase titration on five occasions using a Type 146 multigas calibration system manufactured by Thermo Environmental Instruments Inc. USA. The error caused by zero line drift and change of sensitivity in the measurement period was within 2%. The relative output voltage of the fast sensor was frequently calibrated by a slow response ozone monitor to eliminate the change in sensitivity caused by changing air humidity.

Above ground green biomass (*AGB*) was sampled by cutting the plants above the litter layer > 1 cm in five sampling quadrants along a 5-metre-long transect. The total biomass was separated into dead, dry (yellow, brown) and living (green) parts to understand the dynamics of living (fresh) and senescent (dry) biomass. The biomass was oven-dried at 85 °C for 48 h.

Vegetation height (*h*) was measured at the four corners of the quadrants. Permanent quadrants (40 × 40 cm) located along 5-m long permanent transects were sampled in one- to two-week intervals during summer, autumn, and spring as well as monthly during the winter.

Leaf area index (*LAI*) was estimated from light interception measurements described by Campbell (1986) and Campbell and Norman (1989). Throughout the study we applied the same sampling protocol, measuring device and calculation methodology to estimate *LAI* (for details of *LAI* measurements at the site see Koncz et al. 2015). Therefore, we eliminated the uncertainties which could have been created when using different protocols, devices or analyses (He et al. 2007, Confalonieri et al. 2013). Uncertainties in *LAI* estimation also arise due to the varying leaf area distribution over time in relation to the sun. However, we used the methodology as described by Campbell (1986) and Campbell and Norman (1989). Measured *LAI* was corrected by the ratio of dead/green biomass (*AGB*) to obtain the green fraction.

The measurement methods of all other parameters are listed in Table 1.

2.3 Calculation of Ozone Flux and Dry Deposition Velocity

The 30-min mean ozone fluxes were determined based on the eddy covariance technique using a dry chemiluminescence fast response analyser with a typical precision of 0.3-1.0% between 10 and 100 ppbv at a frequency of f = 10 Hz (Zahn et al. 2012). The absolute ozone concentration was measured by an ozone monitor (types and manufacturers can be seen in Table 1).

We used two methods to calculate turbulent fluxes. The momentum and heat fluxes were calculated according to Nagy et al. (2007), applying the "traditional" planar fit method. These long-term measurements started in 2002.

For the calculation of the ozone flux during the ÉCLAIRE campaign we used the 2D coordinate rotation method for the sonic anemometer measurements. Above flat surfaces both methods can be used with the same precision. The high frequency (10 Hz) data series (3D wind, sonic temperature and ozone voltage signal) were despiked (4 σ), linear detrended, and wind vectors were rotated to the main wind direction (2D rotation, McMillen 1988). The raw relative ozone time series data (U) were shifted considering the lag time at the inlet, based on the maximum correlation of vertical velocity and relative ozone signal. The default time lag (t_{default}) for the maximum covariance was $t_{\text{default}} = 2$ s based on the statistical analysis of the long term flux dataset and a laboratory experiment performed before the measuring campaign (knowing the tube length, diameter and the mean flow rate). The uncertainty of the time lag was a few tenths of seconds. In each time period, we recalculated the time lag by maximizing the eddy covariance. When the calculated maximum time lag, t_{max} was within $t_{\text{default}} \pm 0.5$ s, Φ_{max} was regarded as a valid relative flux (proportional to the flux expressed in the relative unit: mV m s^{-1}), in other cases Φ_{default} with time lag (t_{default}) was chosen as the valid flux (Φ_{max}) (see also Ocheltree and Loescher 2006, Aubinet et al. 2012).

The absolute raw ozone fluxes (F_{raw}) were calculated by the ratio method (Muller et al. 2010) using absolute ozone concentrations (nmol m^{-3}), which does not require the determination of a calibration factor obtained from the relative ozone concentration fluctuation measurements (voltage signals). In this calculation, average ozone concentration and the offset of the fast response ozone sensor (U_{off}) during the flux averaging period are needed to obtain absolute fluxes:

$$F_{\text{raw}} = \frac{\Phi_{\max} c_{\text{avg}}}{U_{\text{avg}} - U_{\text{off}}}, \qquad (1)$$

where c_{avg} and $U_{\text{avg.}}$ are the half-hourly average ozone concentrations from the slow response ozone monitor and the average voltage from the fast response instrument, respectively. The offset (U_{off}) was checked regularly with an active ozone disc by stopping the air flow and it was found to be approximately constant (10 ± 2 mV).

The effect of the density fluctuations generated by the closed-path analyser itself was taken into account by the traditional Webb-Pearman-Leuning (WPL) correction (Webb et al. 1980, Leuning 2007), using the moisture fluctuation term and neglecting the temperature fluctuation term, which is important only for the open path sensors (Rannik et al. 1997, Lee and Massman 2011).

Spectral correction was performed according to two different methodologies.

a) Based on the eddy covariance software package TK3 (Mauder and Foken 2011) corrections were applied for i) inadequate frequency response, ii) sensor line averaging, iii) air sampling through tubes, and iv) flux loss at low frequency due to the limited averaging period.

b) The other empirical method (Ammann et al. 2006) estimates high frequency loss by determining the maximum difference of the relative ogive function of kinematic heat flux covariance $\overline{(w'T')}$ and the ozone flux ($\overline{w'c'}$) as the first step. Secondly, it calculates the spectral correction of the kinematic heat flux according to the TK3 method.

Spectral correction was carried out by using the mean of the two (a and b) methods. In the case of the noisy ogives, when the maximum difference between the ogive functions was higher than 30%, only the TK3 spectral correction (correction a) was used. The final value of ozone flux was denoted as F. The flux calculation program was written in FORTRAN.

Spectral correction depends on stability. Higher relative values were observed during stable stratification. The mean values and standard deviations of the spectral corrections using the methodology of TK3 software and the semi-empirical corrections based on Ammann et al. (2006) are presented in Table 2 for a test period of May 2013. A total of 589 half-hourly measurements were analysed from unstable to stable stratifications in the interval of $-1 < \zeta < 1$.

INSERT HERE TABLE 2

Co-spectral correction (maximum differences between two relative ogive functions for $\overline{w'T'}$ and $\overline{w'c'}$) slightly depends on stability. The mean values and standard deviations are in the same order of magnitude in each stability category (5-7%). Dependence of both types of spectral corrections on stability is similar. The TK3 methodology (TK3 corr. $\overline{w'c'}$) gives higher mean values for each stability category compared to the semi-empirical methodology. The values of spectral corrections are not negligible.

We used a standard flux calculation methodology comparable with other ÉCLAIRE flux sites. The numerical optimisation of the ozone flux ogive function (Sievers et al. 2015) and a more detailed uncertainty analysis of the ozone flux calculation (Zhu et al. 2015) are focuses of near future investigations.

In the present work, the random flux error was estimated as the root mean squared deviation of the covariance function from the zero line within the two tail ranges, which can be calculated as (Nemitz 2014):

$$\delta F = \pm\sqrt{\frac{1}{N}\sum_{\mathrm{i}=1}^{N}\delta_{\mathrm{i}}\rho_{\mathrm{wi}}^{2}}, \quad (2)$$

where ρ_{wi} is the value of the cross-covariance function. The delta function is δ_{i}=1 for those indices (i) which are far from the optimum time lags as: a) (t_{default} – 90 s) < t_{i} < (t_{default} – 30 s), b) (t_{default} + 30 s) < t_{i} < (t_{default} + 90 s), otherwise $\delta_i = 0$. N is the number of samples for which $\delta_i = 1$. In our case $N = 1200$.

The above formula can also be written as:

$$\delta F = \pm\sqrt{0.5\left(\mathrm{std}_{\mathrm{left}}^{2} + \mathrm{avg}_{\mathrm{left}}^{2} + \mathrm{std}_{\mathrm{right}}^{2} + \mathrm{avg}_{\mathrm{right}}^{2}\right)}, \quad (3)$$

where $\mathrm{std}_{\mathrm{left}}$, $\mathrm{avg}_{\mathrm{left}}$, $\mathrm{std}_{\mathrm{right}}$ and $\mathrm{avg}_{\mathrm{right}}$ are the mean and standard deviations of the cross-covariance function of ozone and vertical wind speed using different time delays (t_{i}) on the left and right hand side of the auto-covariance function, respectively.

Dry deposition velocity and random error of deposition were also calculated based on the flux dataset (F) as follows:

$$v_{\mathrm{d}} = \frac{F}{c_{\mathrm{avg}}}, \quad (4)$$

$$\delta v_{\mathrm{d}} = \frac{\delta F}{c_{\mathrm{avg}}}. \quad (5)$$

The uncertainty in the measurements of the average ozone mixing ratio was not taken into account for the calculation. The signals from the fast and slow ozone sensors were recorded separately. We assumed that uncertainties mostly originated from flux measurement errors (Nemitz 2014, Zhu et al. 2015).

Averaged ozone fluxes were calculated for each half-hour period when real signals were received (no error message) both from the ultrasonic anemometer and from the fast response ozone monitor. On the basis of the calculated ozone flux (F) and random flux error (δF), semi-empirical data filtering was applied removing the average half-hour fluxes when: i) $|\delta F| >> |F|$, ii) $F < -10$ nmol m^{-2} s^{-1}, iii) any unrealistic jumping in the values F, δF, and v_{d}, iv) $|F| > 0.5$ nmol m^{-2} s^{-1} and $|\delta F| \geq |F|$. The number of error cases was lower than 5% and occurred mostly in night-time and transient periods.

Spike detection and removal of the raw (10 Hz) data was carried out as suggested by Vickers and Mahrt (1997) and linear detrending was performed afterwards. Possible inaccurate levelling of the sonic anemometer was corrected by the “traditional” planar fit method (Wilczak et al. 2001).

From the corrected raw data, the momentum flux was calculated by the following equation:

$$\tau = \rho\ u_*^2\ = \rho \sqrt{(\overline{u'w'})^2 + (\overline{v'w'})^2}, \qquad (6)$$

where $\overline{u'w'}$ and $\overline{v'w'}$ denotes the covariances of the two horizontal (u, v) components and the vertical (w) component of wind speed.

2.4 Estimation of the Effect of Storage Changes and the Flux Divergence Caused by Chemistry on Calculated Fluxes

Storage changes are an important source of bias in flux estimation, but in the case of low vegetation, uptake is close to the ground surface, hence the storage changes are generally considered to be negligible (Wohlfahrt et al. 2012).

In-canopy chemistry is another sink for ozone (Fuentes et al. 2007). Chemical reactions of ozone, involving biogenic VOCs (Volatile Organic Compounds) should definitely be taken into account in flux calculations, however, they have a dominant role in the case of forested areas (Goldstein et al. 2004). Over grasslands, although the emitted VOCs react with ozone rapidly enough to influence the flux, these emissions are minimal and not measured. Therefore, the strongest potential source of divergence can be the reaction with NO emitted from the soil. However, the influence of NO on the ozone flux profiles is usually weak because the ozone fluxes are typically considerably larger than nitrogen oxide fluxes (Kramm et al. 1995). For a short canopy – even for bare soil – it is generally estimated as negligible, below 1% (Stella et al. 2012). This assumption is supported by the mean soil NO flux (0.025 nmol m^{-2} s^{-1}) measured at our site being two orders of magnitude lower than the ozone flux (measured between 2006 to 2010, Machon et al. 2015). Therefore, the majority of non-stomatal conductance is attributed to the dry deposition and decomposition processes on plant, litter, and soil surfaces.

2.5 Partitioning of Resistance Terms

The reciprocal value of dry deposition velocity equals the sum of aerodynamic, boundary layer, and canopy resistances:

$$\frac{1}{v_\mathrm{d}} = r = r_\mathrm{a} + r_\mathrm{b} + r_\mathrm{c}. \tag{7}$$

To calculate the canopy resistance (r_c) using Eq. (7) we computed the term of ($r_\mathrm{a} + r_\mathrm{b}$) according to Baldocchi and Meyers (1991) and Lamaud et al. (2002) as:

$$r_\mathrm{a} + r_\mathrm{b} = \frac{u}{u_*^2} + \frac{2}{\mathrm{k}u_*}\left(\frac{Sc}{Pr}\right)^{\frac{2}{3}}, \tag{8}$$

where u_* was derived from momentum flux (τ) calculated using ultrasonic anemometer data according to Eq. (6) as described in Section 2.3.

Canopy resistance r_c can be further divided into stomatal (r_st) and non-stomatal (r_nst) terms:

$$\frac{1}{r_\mathrm{c}} = \frac{1}{r_\mathrm{st}} + \frac{1}{r_\mathrm{nst}}, \text{ or } \kappa_\mathrm{c} = \kappa_\mathrm{st} + \kappa_\mathrm{nst}. \tag{9}$$

Non-stomatal conductance (κ_nst) – as the residual of κ_c after subtracting κ_st – represents the bulk conductance of different processes, namely the effect of air chemistry (virtual loss of O_3 by thermal reaction with NO), leaf surface chemistry, as well as deposition to ground level (dead parts of plants, litter) and soil (Byun and Dennis 1995, Fares et al. 2012). Partitioning of κ_c into κ_st and κ_nst cannot be calculated directly. Parameterisation and modelling of stomatal resistance generally use the similarity of ozone flux to other gases like CO_2 or water vapour. Gerosa et al. (2007) proposed an algorithm to calculate the stomatal flux of ozone by the PM and evaporation-resistance approaches using measured water vapour flux. Those formulae assume equivalence between the stomatal water vapour flux (E_t) and the total water vapour flux used for closed canopy with negligible soil evaporation. However, for our open canopy (LAI_mean = 0.5) water vapour flux consists not only of stomatal transpiration but also of evaporation. Shuttleworth and Wallace (1985) described a one-dimensional model (see also in Hu et al. 2009) to partition the evaporation (E_e) and transpiration (E_t) terms (all the equations shown below are based on SW model, unless stated otherwise):

$$\lambda E = \lambda E_\mathrm{e} + \lambda E_\mathrm{t} = \mathrm{C_c} PM_\mathrm{c} + \mathrm{C_s} PM_\mathrm{s}, \tag{10}$$

where

$$PM_\mathrm{c} = \frac{\Delta R + (\rho c_\mathrm{p} D - \Delta r_\mathrm{ac} R_\mathrm{s})/(r_\mathrm{aa} + r_\mathrm{ac})}{\Delta + \gamma[1 + r_\mathrm{sc}/(r_\mathrm{aa} + r_\mathrm{ac})]}, \tag{11}$$

and

$$PM_\mathrm{s} = \frac{\Delta R + [\rho c_\mathrm{p} D - \Delta r_\mathrm{as}(R - R_\mathrm{s})]/(r_\mathrm{aa} + r_\mathrm{as})}{\Delta + \gamma[(1 + r_\mathrm{ss}/(r_\mathrm{aa} + r_\mathrm{as})]}. \tag{12}$$

Radiation terms are expressed as (Hu et al. 2009):

$$R = R_{\mathrm{n}} - G, \tag{13}$$

$$R_{\mathrm{s}} = R_{\mathrm{ns}} - G, \tag{14}$$

and

$$R_{\mathrm{ns}} = R_{\mathrm{n}}\,\mathrm{e}^{-0.6\,LAI}. \tag{15}$$

The soil heat flux was estimated according to Hillel (1998) combining the time lag and damping deep methods, using the measured soil wetness (θ) and temperature (t_s) at two upper depths (–0.03; –0.30 m). When soil physical measurements were not available (less than 5% of all the cases) G was estimated from the mean ratio of calculated soil heat flux by Hillel (1998) and the measured net radiation:

$$G = 0.1 \times R_{\mathrm{n}}. \tag{16}$$

Canopy and surface resistance coefficients (17)-(21) were calculated (Shuttleworth and Wallace 1985) as:

$$\mathrm{C_c} = \frac{1}{1+\left[\frac{\rho_{\mathrm{c}}\rho_{\mathrm{a}}}{\rho_{\mathrm{s}}\,(\rho_{\mathrm{c}}+\rho_{\mathrm{a}})}\right]} \tag{17}$$

and

$$\mathrm{C_s} = \frac{1}{1+\left[\frac{\rho_{\mathrm{s}}\rho_{\mathrm{a}}}{\rho_{\mathrm{c}}\,(\rho_{\mathrm{s}}+\rho_{\mathrm{a}})}\right]}, \tag{18}$$

where

$$\rho_{\mathrm{a}} = (\Delta + \gamma) r_{\mathrm{aa}}, \tag{19}$$

$$\rho_{\mathrm{c}} = (\Delta + \gamma) r_{\mathrm{ac}} + \gamma r_{\mathrm{sc}}, \tag{20}$$

$$\rho_{\mathrm{s}} = (\Delta + \gamma) r_{\mathrm{as}} + \gamma r_{\mathrm{ss}}. \tag{21}$$

The resistances in the SW model were estimated as follows: r_{aa} and r_{as} were calculated according to Shuttleworth and Wallace (1985) from the parameters z, d, z_0, h, k, u, and n (assuming that $d = 0.63 \times h$ and $z_0 = 0.13 \times h$, Shuttleworth and Wallace 1985). For a fully developed crop ($LAI > 4$):

$$r_{\mathrm{aa}}(\alpha) = \frac{\ln\left(\frac{z-d}{z_0}\right)}{\mathrm{k}^2 u}\left\{\ln\frac{z-d}{h-d} + \frac{h}{\mathrm{n}(h-d)}\, e^{\mathrm{n}\left[1-\frac{(d+z_0)}{h}\right]} - 1\right\}, \tag{22}$$

and

$$r_{\mathrm{as}}(\alpha) = \frac{\ln\left(\frac{z-d}{z_0}\right)}{\mathrm{k}^2 u}\,\frac{h}{\mathrm{n}(h-d)}\left[e^{\mathrm{n}} - e^{\mathrm{n}\left(1-\frac{d+z_0}{h}\right)}\right]. \tag{23}$$

For bare soil:

$$r_{\mathrm{aa}}(0) = \frac{\ln^2\left(\frac{z}{z_0'}\right)}{\mathrm{k}^2 u} - r_{\mathrm{as}}(0), \tag{24}$$

and

$$r_{\mathrm{as}}(0) = \frac{\ln\frac{z}{z_0'}\ln\frac{(d+z_0)}{z_0'}}{\mathrm{k}^2 u}, \tag{25}$$

where $z_0' = 0.01$m.

For a canopy with $0 < LAI < 4$ (as in our case) the two resistance terms in the model are (Shuttleworth and Wallace 1985):

$$r_{\mathrm{aa}} = \frac{LAI\, r_{\mathrm{aa}}(\alpha)}{4} + \frac{(4-LAI) r_{\mathrm{aa}}(0)}{4}, \tag{26}$$

and

$$r_{\mathrm{as}} = \frac{LAI\, r_{\mathrm{as}}(\alpha)}{4} + \frac{(4-LAI) r_{\mathrm{as}}(0)}{4}, \tag{27}$$

furthermore (according to Shuttleworth and Wallace 1985):

$$r_{\mathrm{ac}} = \frac{r_{\mathrm{bv}}}{2\, LAI}, \tag{28}$$

and

$$r_{\mathrm{sc}} = \frac{r_{\mathrm{mst}}}{2\, LAI}. \tag{29}$$

The r_{ss} resistance term was derived according to Hu et al. (2009) as:

$$r_{\mathrm{ss}} = \mathrm{b}_1 \left(\frac{\theta_{\mathrm{s}}}{\theta}\right)^{\mathrm{b}_2} + \mathrm{b}_3, \tag{30}$$

where $\mathrm{b}_1 = 2.63$ s m^{-1}, $\mathrm{b}_2 = 1.32$, and $\mathrm{b}_3 = 4.87$ s m^{-1}. Empirical constants (b_1, b_2, and b_3) were applied for a temperate steppe similar to our site, optimised with a Monte Carlo simulation (Hu et al., 2009) We also tested wide intervals of b_1, b_2, and b_3 constants for all types of surface (b_1 = 1-5; b_2 = 1-5; b_3 = 1-500). The variation of b_1 (1-5), b_2 (1-2.6), and b_3 (1-5) caused 1.8% and 0.97% variances in the calculated transpiration and evaporation terms, respectively. The increase of b_2 and b_3 to the upper limit (5 and 500, respectively) resulted in a 40-70% increase in the latent heat flux from the canopy and a proportional decrease in the latent heat flux from the soil. In parallel, the correlation also decreased between the calculated and measured latent heat flux towards the upper limit. We obtained maximum correlation by using $\mathrm{b}_1 = 2.63$ s m^{-1}, $\mathrm{b}_2 = 1.32$, $\mathrm{b}_3 = 4.87$ s m^{-1}, hence we accepted these as optimised values.

After calculation of the *PM* and C terms stomatal transpiration ($\mathrm{C_c}PM_{\mathrm{c}}$) and soil evaporation ($\mathrm{C_s}PM_{\mathrm{s}}$) can be separated. Using the calculated transpiration rate the stomatal conductance can be computed by inverting the PM equation as suggested by Lamaud et al. (2002):

$$\kappa_{\mathrm{st}} = \frac{D_{\mathrm{O_3}}}{D_{\mathrm{w}}} \frac{\frac{E_{\mathrm{t}}}{\delta}}{1+\frac{E_{\mathrm{t}}}{\delta}(r_{\mathrm{a}}+r_{\mathrm{b}})\left(\frac{\beta\Delta}{\gamma}-1\right)}, \tag{31}$$

where

$$\delta = \rho_{\mathrm{vs}} - \rho_{\mathrm{v}};\ \rho_{\mathrm{vs}} = \frac{e_{\mathrm{s}}}{R_{\mathrm{w}}T}, \tag{32}$$

$$\rho_{\mathrm{v}} = \frac{e}{R_{\mathrm{w}}T};\ e = e_{\mathrm{s}}RH, \tag{33}$$

$$e_{\mathrm{s}} = 611 \times 10^{\frac{\mathrm{a}t}{\mathrm{b}+t}} \tag{34}$$

where a = 7.5/9.5; b = 237.3/265.5 °C for water/ice, respectively (Magnus-Tetens formula), and

$$s = \frac{e_{\mathrm{s}}\lambda}{R_{\mathrm{w}}T^2}, \tag{35}$$

$$\gamma = \frac{c_{\mathrm{p}}p}{0.6215\ \lambda}, \tag{36}$$

where 0.6215 is the molecular weight ratio of water to dry air.

Stomatal flux was derived according to Mészáros et al. (2009) by using the different resistances as:

$$-F_{\mathrm{st}} = c\ \kappa_{\mathrm{st}}\left(\frac{r_{\mathrm{c}}}{r}\right). \tag{37}$$

3 Results

3.1 Validation of the Model

Direct validation of the coupled SW-PM model is not possible due to the lack of measured stomatal conductance. The last but one step in the modelling is the calculation of water vapour flux before partitioning it into evaporation and transpiration terms. Hence, we can compare the measured and modelled water vapour fluxes. Fig. 1 shows the regression and correlation between measured and modelled water vapour fluxes for the whole period. The regression parameters suggest a close relationship between the measured and modelled values.

INSERT HERE FIGURE 1

3.2 Response of model output to the change of main input parameters

We examined how predicted stomatal conductance responds to the change of the most effective physical parameters, such as leaf area index (*LAI*), available energy input (*R*), and relative humidity (*RH*) of air (Fig. 2). We tested these variables in the model by changing the value of the investigated variable whilst keeping the others constant. The increase of the available energy input increased the stomatal conductance along a logarithmic scale (left panel).

Relative humidity slightly increased the stomatal conductivity at low *RH* values, while at higher *RH*, an exponential increase of κ_{st} was observed (middle panel). The strongest dependence was observed in the case of *LAI* (right panel). At lower *LAI* values the model output was quite sensitive to an increase of *LAI,* following a saturation curve towards the high leaf area indices. As it is generally accepted, above *LAI* = 4 the vegetation is regarded as fully developed. In this case soil evaporation does not make a significant contribution to latent heat flux, hence the share of the evaporation term in evapotranspiration decreases, leading to $\lambda E \cong \lambda E_{\mathrm{t}}$. Therefore, the increase of κ_{st} above *LAI* = 4 is weak

INSERT HERE FIGURE 2

3.3 Daily Fluxes of Ozone

Half-hourly average ozone fluxes were calculated according to Eq. 1. Due to the uncertainty of the observations, caused mainly by the lack of turbulence during night hours, the data set was filtered as described in Section 2.3. The seasonal variation of the averaged daily fluxes is illustrated in Fig. 3. Characteristic differences can be seen between the fluxes measured in the growing and dormant periods. It is evident that in the summer half-year (April-September) the role of stomatal uptake is more relevant compared to the dormant season. In the vegetative period, the magnitude of the fluxes greatly depends – among others – on the green biomass, and in particular, on *LAI.* This can be seen in Fig. 4 where two 12-day periods (see 3.4 for details) were compared with different leaf area indices. It can be noted – as described in detail in Section 3.4 – that August 2012 was a dry period in contrast to May 2013 when there was no water limitation affecting the stomatal ozone fluxes (Mészáros et al. 2009). Differences between *LAI* and moisture characteristics resulted in significantly higher total and stomatal ozone fluxes in May 2013.

INSERT HERE FIGURE 3

INSERT HERE FIGURE 4

3.4 Partitioning Stomatal and Non-stomatal Conductance

The half hourly averages of dry deposition velocities were calculated according to Eq. 4. The canopy conductance κ_c was derived from Eq. (7) and (8). After partitioning the transpiration and evaporation terms according to Eq. (10)-(30), stomatal conductances were calculated by Eq. (31)-(36). At night, the radiation terms have zero or negative values in Eq. (11) ($R_g = 0$ and R, $R_s < 0$ W m^{-2}) and stomata are practically closed (as it is supposed below in this section); hence, r_{st} is close to infinity and the calculated r_c refers to the non-stomatal resistances, i.e. $r_c = r_{nst}$ or $\kappa_c = \kappa_{nst}$ according to Eq. (9).

To evaluate the general pattern of the daily variation of the stomatal and the non-stomatal conductances, we calculated the bulk daily course of these parameters for the total measurement period of August 2012 to January 2014 (Fig. 5), separately for the summer (April-September) and winter (October-March) half-years.

INSERT HERE FIGURE 5

Night-time transpiration and stomatal conductance were regarded as zero. The summer half-year includes the majority of the growing season; however, growth of above-ground green biomass was also observed at the beginning and at the end of the winter half-year. As it can be seen from the graphs, stomatal conductance is roughly two times higher in the summer half-year. Non-stomatal deposition dominates throughout the day in both seasons, showing a less even pattern than stomatal conductance owing to the great number of physical parameters governing non-stomatal deposition through many different processes. Not only soil deposition, which is dominant for sparse vegetation (characterized by low *LAI* as observed e.g. by Stella et al. 2013), but also wet leaf surface chemistry, i.e. cuticular deposition, is a sink of ozone. It has to be mentioned here that throughout the modelling period, the observed mean leaf area index was $LAI = 0.5$. The share of stomatal, non-somatal, and canopy bulk conductances are of the same order of magnitude compared to other investigations (Kelliher et al. 1995, Pio et al. 2000, Tuovinen et al. 2004).

A t-test was applied for medium *LAI* cases when the expected values of κ_{st} and κ_{nst} are similar. In the range of $LAI = 1.0$-2.2 the means of the two conductances were 0.23 and 0.25 cm s^{-1}, respectively. Only daytime cases were taken into account since at night $\kappa_{st} = 0$. The parameters of the t-test were $t = -2.06$, $t_{0.05} = 1.96$, $p = 0.04$, and $n = 1011$. Since $|t| > t_{0.02}$ ($p < 0.05$) the two datasets are significantly different.

The combined effect of low moisture availability and sparse vegetation on the stomatal uptake, calculated by Eq. (37), is well represented by the substantial difference in stomatal flux in the dry season with *LAI* = 0.25 (Fig. 4, left panel) and in the wet period with leaf area indices being 4-times higher (right panel), as it can be followed in Table 3.

For a more detailed examination of stomatal and non-stomatal conductances in the growing season, we analysed two 12-day observation periods in August 2012 and May 2013 (Table 3). The criteria for selection were: i) a continuous dataset, ii) as large a difference between mean *LAI* as possible (1.05 vs. 0.25), 3) the period is part of the growing season.

INSERT HERE TABLE 3

The first investigated period (12-23 August 2012) was a typical, dry summer season with no rain. The daily maximum of global and net radiation was 770-890 W m^{-2} and 550-575 W m^{-2}, respectively (except 12 August, which was a cloudy day), and the daily maximum values of the latent heat fluxes did not exceed 80-130 W m^{-2}. The typical daytime Bowen-ratio was $\beta = 1.4$. The mean leaf area index (*LAI*) was 0.25 with a mean above-ground green biomass (*AGB*) of 3.2 g m^{-2}; other mean physical parameters in August were *RH* = 57%; leaf wetness *LW* = 11%, and air temperature $t_a = 20$ °C.

The second period (2-13 May 2013) was a typical late spring period with 32 mm of precipitation on 4 rainy days. There was a large variation in the daily maximum values of the global and net radiations. They varied within 200-865 W m^{-2} and 100-600 W m^{-2}, respectively. The typical daytime Bowen-ratio values were $\beta = 0.25$-0.40. In this period, there was no water limitation. These 12 days can be characterized as: mean *LAI* = 1.05; *AGB* (green) = 96 g m^{-2}; *RH* = 75%; *LW* = 25%, and $t_a = 17$ °C.

Conductances and fluxes were selected according to global radiation into daytime (R_g, $R >$ 0 W m^{-2}) and night ($R_g = 0$ and $R <$ 0 W m^{-2}) groups. Night-time transpiration was regarded as negligible with zero stomatal conductance.

Although incomplete closing of stomata has been observed during the night (Caird et al. 2007), very little is understood about this phenomenon. At night the main governing factors for transpiration, e.g. the water vapour pressure difference between leaves and air as well as atmospheric mixing, are much lower than during the daytime; hence, transpiration is lower by one order of magnitude, it represents only 5-15% of the daytime rate. The magnitude of stomatal exchange can also be estimated by comparing the ratio of the mean calculated transpiration terms (E_t) during the daytime (R_g and $R >$ 0 W m^{-2}) and at night ($R_g = 0$ and $R <$ 0 W m^{-2}). They were 1.53×10^{-5} (day), 0.0269×10^{-5} kg m^{-2} s^{-1} (night) and 3.28×10^{-5} (day),

0.336×10^{-5} kg m^{-2} s^{-1} (night) in August 2012 and May 2013, respectively. The ratios of day to night transpiration rates were 56.7 in August (mean *LAI* = 0.25) and 9.76 in May (mean *LAI* = 1.05). Similarly, the day to night stomatal conductivity ratio for water vapour calculated as $\kappa_w = E_t/\rho_v$ was 51.4 in August 2012 and 16.7 in May 2013. These values verify the at least one order of magnitude lower transpiration rate at night especially for the examined ecosystem. Therefore, in this study we considered the night-time transpiration rate and stomatal conductance as negligible.

The first period is represented by a low leaf area index of 0.25. In the second period the vegetation is more developed with an average *LAI* = 1.05 (Table 3). There are further differences between the two periods; namely, in May 2013 the relative humidity and the leaf wetness were higher and a large increase was observed in the mass of above-ground green biomass. Evidently, there are parallel increases in the number of stomata with increasing *LAI* and *AGB* (green) which is reflected in the 8.5-times higher stomatal conductivity in the daytime in May compared to August when lower *LAI* values and drought were observed. There is a factor of 2 in the non-stomatal conductance between lower and higher *LAI* situations, showing the importance of cuticular deposition, and the relatively wet climate regime in May 2013 that favours not only cuticular uptake but also deposition processes to wet surfaces. In the season represented by *LAI* = 0.25 the ratio of κ_{nst}/κ_{st} is around 4-5 and when the *LAI* reaches unity (= 1), the daytime ratio of these two parameters becomes the same in magnitude.

A similar pattern can be seen in the total ozone flux and in the stomatal flux in Table 3. While total ozone flux has doubled due to growth of *LAI* and other factors, stomatal flux increased by a factor of 5. These variations can also be observed in Fig. 6 and 7, where the variation of stomatal and canopy conductances as well as total and stomatal ozone fluxes are illustrated together.

INSERT HERE FIGURE 6

INSERT HERE FIGURE 7

When vegetation is completely covered by snow there appears to be no stomatal activity. Table 3 shows this situation on five selected days (15; 16; 26; 27; 28 March 2013) with the highest snow depth episodes (12-16 cm) completely covering the 5-7 cm tall vegetation. In this case $\kappa_{nst} = \kappa_c$ refers to the ozone surface conductance to snow. Conductances were small, approximately 0.03 cm s^{-1} on average (in agreement with earlier observations, e.g. by Wesely et al. 1980), practically independent of the period of the day.

During control days in the same month (12; 13; 19; 20; 21 March, 2013) maximum daily temperatures ranged between 10 and 15 °C, net radiations were below 200 W m^{-2}), the vegetation was still free of snow, but regarding the dormant season stomatal conductance was negligibly small.

Interestingly non-stomatal conductivity is as high in magnitude as in the following May. This phenomenon can be explained by the wet surfaces as illustrated in Table 3, by the high relative humidity and soil water content, indicating the importance of surface loss processes in the non-stomatal deposition of ozone.

4 Summary and Conclusion

We partitioned canopy conductance into different parts (non-stomatal and stomatal) by calculating the stomatal conductance separately. For well-developed vegetation ($LAI > 4$) evaporation in the evapotranspiration process is practically negligible, hence transpiration can be used to calculate the stomatal conductance of water vapour and ozone, using the similarity between them described by the PM theory. In the case of low, sparse vegetation ($LAI < 4$), evaporation is no longer negligible; therefore, E has to be partitioned into E_t and E_e to estimate stomatal conductance for water and for ozone using the transpiration term in the PM equation. We found that the coupled SW and PM model can simulate and partition stomatal and non-stomatal conductances over short, low, and sparse vegetation, where evaporation is of the same magnitude or even more significant than transpiration. Our result suggests that the non-stomatal part is highly significant in controlling total ozone deposition to sparse vegetation.

Acknowledgements The authors are grateful for the permission of the Management of Kiskunság National Park to conduct the studies on the territory of the park in Bugacpuszta. This work has been supported by the NitroEurope EU 6th FP (017841), the Animal Change EU 7th FP (266018), the ÉCLAIRE EU 7th FP (282910), the Hungarian Scientific Research Foundation (OTKA, project No. NN109679 and K83909) and the Research Centre of Excellence, Hungary (8526-5/2014/TUDPOL) programs. Special thanks for language editing by Iain Coulthard.

References

Amann M, Bertok I, Borken-Kleefeld J, Cofala J, Heyes C, Höglund-Isaksson L, Klimont Z, Nguyen B, Posch M, Rafaj P, Sander R, Schöpp W, Wagner F, Winiwarter W (2011) Cost-effective control of air quality and greenhouse gases in Europe: modeling and policy applications. Environmental Model Softw 26:1489–1501

Ammann C, Brunner C, Spirig A, Neftel A (2006) Technical note: Water vapour concentration and flux measurements with PTR-MS. Atmos Chem Phys 6 4643:4651

Aubinet M, Papale D, Vesala T (2012) Eddy covariance A Practical Guide to Measurement and Data Analysis. Springer Dordrecht, Heidelberg, London, New York, 438 pp

Baldocchi DD, Meyers TP (1991) Trace gas exchange above the floor of a deciduous forest 1 Evaporation and CO_2 efflux. J Geophys Res D: Atmos 96:7271–7285

Byun DW, Dennis R (1995) Design artifacts in Eulerian air quality models: evaluation of the effects of layer thickness and vertical profile correction on surface ozone concentrations. Atmos Environ 29 105:126

Caird MA, Richards JH, Donovan LA (2007) Nighttime stomatal conductance and transpiration in C_3 and C_4 Plants. Plant Physiol 143 4:10

Campbell GS (1986) Extinction coefficients for radiation in plant canopies calculated using an ellipsoidal inclination angle distribution. Agric For Meteorol 36 317:321

Campbell GS, Norman JM (1989) The description and measurement of plant canopy structure. In: G Russell, B Marshall, and PG Jarvis (Eds), Plant Canopies: Their Growth, Form, and Function Society for Experimental Biology 31, Cambridge University Press, Cambridge, pp 1–18

Colette A, Granier C, Hodnebrog Ø, Jakobs H, Maurizi A, Nyiri A, Rao S, Amann M, Bessagnet B, D'Angiola A, Gauss M, Heyes C, Klimont Z, Meleux F, Memmesheimer M, Mieville A, Rouïl L, Russo F, Schuchtl S, Simpson D, Stordal F, Tampieri F, Vrac M (2012) Future air quality in Europe: a multi-model assessment of projected exposure to ozone. Atmos Chem Phys 12 10613:10630

Confalonieri R, Foi M, Casa R, Aquaro S, Tona E, Peterle M, Boldini A, Carli GD, Ferrari A, Finotto G et al. (2013) Development of an app for estimating leaf area index using a smartphone. Trueness and precision determination and comparison with other indirect methods. Comput Electron Agric 96 67:74

Coyle M, Nemitz E, Storeton-West R, Fowler D, Cape JN (2009) Measurements of ozone deposition to a potato canopy. Agric For Meteorol 149 655:666

Emberson LD, Ashmore MR, Cambridge HM, Simpson D, Tuovinen J-P (2000) Modelling stomatal ozone flux across Europe. Environ Pollut 109 403:413

Fares S, Weber R, Drew J-H Karlik GJ, Goldstein AH (2012) Ozone deposition to an orange orchard: partitioning between stomatal and non-stomatal sinks. Environ Pollut 169 258:266

Fuentes JD, Wang D, Bowling DR, Potosnak M, Monson RK, Goliff WS, Stockwell WR (2007) Biogenic hydrocarbon chemistry within and above a mixed deciduous forest. J Atmos Chem 56 165:185

Gerosa G, Derghi F, Cieslik, S (2007) Comparison of different algorithms for stomatal ozone flux determination from micrometeorological measurements. Water Air Soil Pollut 179 309:321

Gerosa G, Mereu S, Finco A, Marzuoli, R (2012) Stomatal conductance modeling to estimate the evapotranspiration of natural and agricultural ecosystems. In: A Irmak (Ed), Evapotranspiration - Remote Sensing and Modeling, InTech, Rijeka, Shanghai

Goldstein AH, McKay M, Kurpius MR, Schade GW, Lee A, Holzinger R, Rasmussen RA (2004) Forest thinning experiment confirms ozone deposition to forest canopy is dominated by reaction with biogenic VOCs. Geoph Res Lett 31 L22106

Grantz DA, Zhang XJ, Massman WJ, den Hartog, G (1995) Effect of stomatal conductance and surface wetness on ozone deposition in field-grown grape. Atmos Environ 29 3189:3198

He Y, Guo X, Wilmshurst JF (2007) Comparison of different methods for measuring leaf area index in a mixed grassland. Can J of Plant Sci 87 803:813

Hillel D (1998) Environmental Soil Physics Academic Press, San Diego, USA CA, pp 309:316

Hu Z, Yu G, Zhou Y, Sun X, Li Y, Shi P, Wang Y, Song A, Zheng Z, Zhang L, Li S (2009) Partitioning of evapotranspiration and its controls in four grassland ecosystems: Application of a two-source model. Agric For Meteorol 149 1410:1420

Jarvis PG (1976) The interpretation of the variations in leaf water potential and stomatal conductance found in canopies in the field. Phil Trans R Soc Lon B 373 593:610

Kelliher FM, Leuning R, Raupach MD, Schulze E-D (1995) Maximum conductances for evaporation from global vegetation types. Agric For Meteorol 73 l:l 6

Koncz P, Besnyői V, Csathó AI, Nagy J, Szerdahelyi T, Tóth Zs, Pintér K, Balogh J, Nagy Z, Bartha S (2014) Effect of grazing and mowing on the microcoenological composition of a semi-arid grassland in Hungary. Appl Ecol Environ Res 12 563:575

Koncz P, Balogh J, Papp M, Hidy D, Pintér K, Fóti Sz, Klumpp K, Nagy Z (2015) Higher soil respiration under mowing than under grazing explained by biomass differences. Nutr Cycl Agroecosys 103 201:215

Kramm G, Dlugi R, Dollard GJ, Foken T, Mölders N, Müller H, Seiler W, Sievering H. (1995) On the dry deposition of ozone and reactive nitrogen species. Atmos Environ 29 3209:3231

Lamaud E, Carrara A, Brunet Y, Lopez A, Druilhet, A (2002) Ozone fluxes above and within a pine forest canopy in dry and wet conditions. Atmos Environ 36 77:88

Lamaud E, Loubet B, Irvine M, Stella P, Personne E, Cellier P (2009) Partitioning of ozone deposition over a developed maize crop between stomatal and non-stomatal uptakes, using eddy-covariance flux measurements and modelling. Agric For Meteorol 149 1385:1396

Lee X, and Massman WJ (2011) A Perspective on thirty years of the Webb, Pearman and Leuning Density Corrections. Bound-Layer Meteorol 139 37:59

Leuning R (2007) The correct form of the Webb, Pearman and Leuning equation for eddy fluxes of trace gases in steady and non-steady state, horizontally homogeneous flows. Bound-Layer Meteorol, 123, 263–267

Machon A, Horváth L, Weidinger T, Grosz B, Pintér K, Tuba Z, Führer E (2010) Estimation of net nitrogen flux between the atmosphere and a semi-natural grassland ecosystem in Hungary. Eur J Soil Sci 61 631:639

Machon A, Horváth L, Weidinger T, Grosz B, Móring A, Führer E. (2015) Measurement and modeling of N-balance between atmosphere and biosphere over a grazed grassland (Bugacpuszta) in Hungary. Water Air Soil Pollut 226:27

Massman WJ (2004) Toward an ozone standard to protect vegetation based on effective dose: a review of deposition resistances and a possible metric. Atmos Environ 38 2323:2337

Mauder M, Foken T (2011) Documentation and Instruction Manual of the Eddy-Covariance Software Package. TK3 Universität Bayreuth Abt Mikrometeorologie Arbeitsergebnisse Nr 46, Bayreuth

McMillen RT (1988) An eddy-correlation technique with extended applicability to non-simple terrain. Bound-Layer Meteorol 43 231:245

Mészáros R, Szinyei D, Vincze Cs, Lagzi I, Turányi T, Haszpra L, Tomlin AS (2009) Effect of the soil wetness state on the stomatal ozone fluxes over Hungary. Int J Environ Pollut 36 180:194

Mills G, Pleijel H, Braun S, Büker P, Bermejo V, Calvo E, Danielsson H, Emberson L, Fernández IG, Grünhage L, Harmens H, Hayes F, Karlsson P-E, Simpson D (2011) New stomatal flux-based critical levels for ozone effects on vegetation. Atmos Environ 45 5064:5068

Muller JBA, Percival CJ, Gallagher MW, Fowler D, Coyle M, Nemitz E (2010) Sources of uncertainty in eddy covariance ozone flux measurements made by dry chemiluminescence fast response analysers. Atmos Meas Tech 3 163:176

Musselman RC, Lefohn AS, Massman WJ, Heath RL (2006) A critical review and analysis of the use of exposure- and flux-based ozone indices for predicting vegetation effects. Atmos Environ 40 1869:1888

Nagy Z, Pintér K, Czóbel S, Balogh J, Horváth L, Fóti S, Barcza Z, Weidinger T, Csintalan Z, Dinh NQ, Grosz B, Tuba Z (2007) The carbon budget of a semiarid grassland in a wet and a dry year in Hungary. Agricult Ecosys Environ 121 21:29

Nemitz E (2014) Analysis of the EC cross covariance function for lag and error determination (Methodology of the Swiss Agroscope Group, Ch Ammann; edited by E Nemitz, CEH, Edinburgh) Personal communication

Pio CA, Feliciano MS, Vermeulen AT, Sousa EC (2000): Seasonal variability of ozone dry deposition under southern European climate conditions. Atmos Environ 34 195:205

Ocheltree TW, Loescher HW (2006) Design of the AmeriFlux Portable Eddy Covariance System and Uncertainty Analysis of Carbon Measurements. J Atmos Ocean Tech 24 1386:1462

Rannik Ü, Vesala T, Keskinen R (1997) On the damping of temperature fluctuations in a circular tube relevant to the eddy covariance measurement technique. J Geophys Res Atmos 102 12789:12794

Rummel U, Ammann C, Kirkman GA, Moura MAL, Foken T, Andreae MO, Meixner FX (2007) Seasonal variation of ozone deposition to a tropical rain forest in southwest Amazonia. Atmos Chem Phys 7 5415:5435

Schurath U, Speuser W, Schmidt R (1991) Principle and application of a fast sensor for atmospheric ozone. Fresen J Anal Chem 340 544:547

Sievers J, Papakyriakou T, Larsen SE, Jammet MM, Rysgaard S, Sejr MK, Sørensen LL (2015) Estimating surface fluxes using eddy covariance and numerical ogive optimization. Atmos Chem Phys 15 2081:2103

Shuttleworth WJ, Wallace JS (1985) Evaporation from sparse crops – an energy combination theory. Q J R Meteorol Soc 111 839:855

Stella P, Loubet B, Laville P, Lamaud E, Cazaunau M, Laufs S, Bernard F, Grosselin B, Mascher N, Kurtenbach R, Mellouki A, Kleffmann J, Cellier P (2012) Comparison of methods for the determination of NO-O_3-NO_2 fluxes and chemical interactions over a bare soil. Atmos Meas Tech 5 1241:1257

Stella P, Personne E Lamaud E, Loubet B, Trebs I, Cellier P (2013) Assessment of the total, stomatal, cuticular, and soil 2 year ozone budgets of an agricultural field with winter wheat and maize crops. J Geophys Res Biogeosci 118 1120:1132

Sutton M, Howard C, Nemitz E (2013) "ÉCLAIRE” - Effects of Climate Change on Air Pollution Impacts and Response Strategies for European Ecosystems - First Periodic Report 01/10/2011 to 31/03/2013 NERC Open Research Achive, http://noranercacuk/505863/

Tuovinen J-P, Ashmore MR, Emberson LD, Simpson D (2004) Testing and improving the EMEP ozone deposition module. Atmos Environ 38 2373:2385

Vickers D, Mahrt L (1997) Quality control and flux sampling problems for tower and aircraft data. J Atmos Ocean Tech 14 512:526

Wang YP, Leuning R (1998) A two-leaf model for canopy conductance, photosynthesis and partitioning of available energy I: Model description and comparison with a multi-layered model. Agric For Meteorol 91 89:111

Webb EK, Pearman G, Leuning R (1980) Correction of flux measurements for density effects due to heat and water vapour transfer. Q J R Meteorol Soc 106 85:100

Wesely ML, Cook DR, Williams RM (1980) Field measurement of small ozone fluxes to snow, wet bare soil, and lake water. Bound-Layer Meteorol 20 459:471

Wilczak JM, Oncley SP, Stage SA (2001) Sonic anemometer tilt correction algorithms. Bound-Layer Meteorol 99 127:150

Wohlfahrt G, Klumpp K, Soussana, JF (2012) Eddy covariance measurements over grasslands In: M Aubinet et al (Eds), Eddy Covariance: A Practical Guide to Measurement and Data Analysis, Springer Atmospheric Sciences. Springer Science+Business Media BV, pp 333:344

Zahn A, Weppner J, Widmann H, Schlote-Holubek K, Burger B, Kühner T, Franke H (2012) A fast and precise chemiluminescence ozone detector for eddy flux and airborne application. Atmos Meas Tech 5 363:375

Zhu Z, Zhao F, Voss L, Xu L, Sun X, Yoi G, Meixner FX (2015) The effects of different calibration and frequency response correction methods on eddy covariance ozone flux measured with a dry chemiluminescence analyzer. Agric For Meteorol 213 114:125

Figure

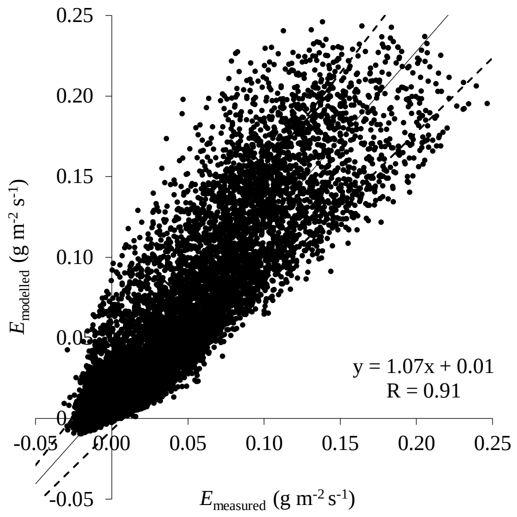

0.25
0.20
0.15
0.10
0.05
0
-0.05
-0.05
0.00
0.05
0.10
0.15
0.20
0.25
E modelled (g m-2 s-1)
E measured (g m-2 s-1)
y = 1.07x + 0.01
R = 0.91

Figure

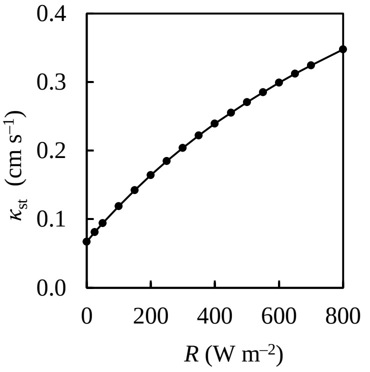

0.4
0.3
0.2
0.1
0.0
κst (cm s−1)
0
200
400
600
800
R (W m−2)
1.0
0.8
0.6
0.4
0.2
0.0
κst (cm s−1)
0
20
40
60
80
100
RH (%)
0.5
0.4
0.3
0.2
0.1
0.0
κst (cm s−1)
0
1
2
3
4
5
6
7
LAI

Figure

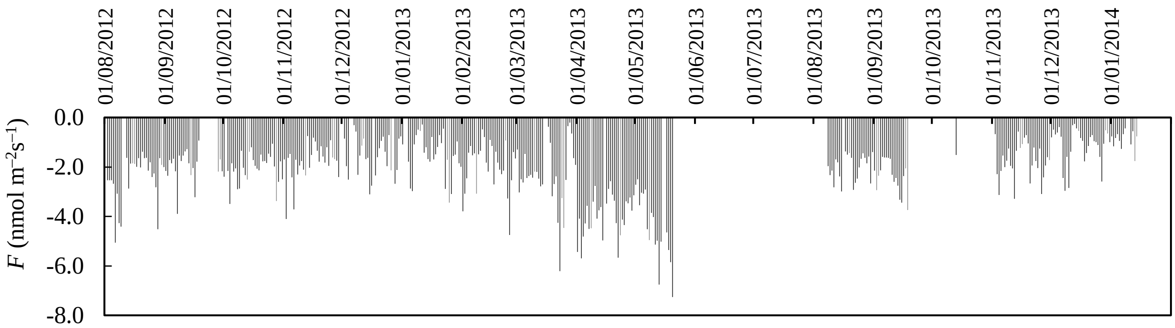
01/08/2012
01/09/2012
01/10/2012
01/11/2012
01/12/2012
01/01/2013
01/02/2013
01/03/2013
01/04/2013
01/05/2013
01/06/2013
01/07/2013
01/08/2013
01/09/2013
01/10/2013
01/11/2013
01/12/2013
01/01/2014
0.0
-2.0
-4.0
-6.0
-8.0
F (nmol m-2s-1)

Figure

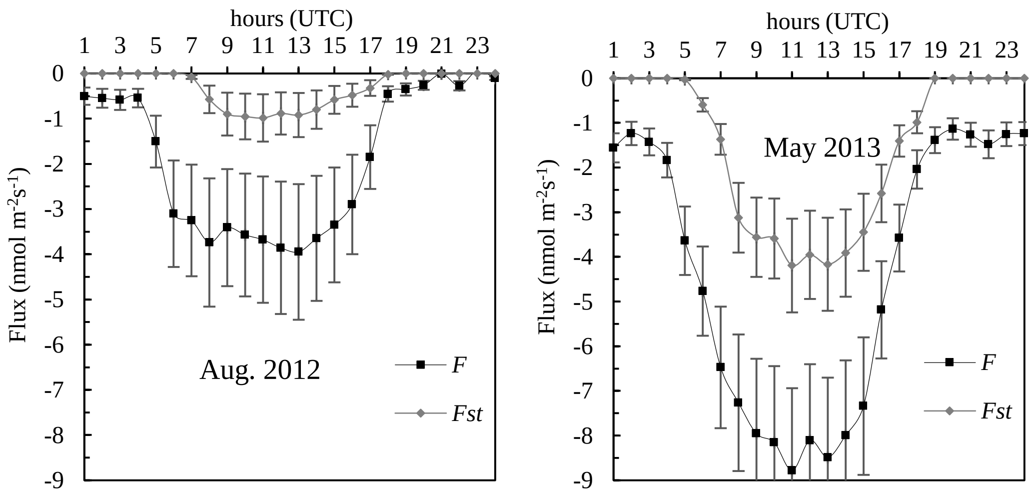
hours (UTC)
1 3 5 7 9 11 13 15 17 19 21 23
0 -1 -2 -3 -4 -5 -6 -7 -8 -9
Flux (nmol m-2s-1)
Aug. 2012
F
Fst
hours (UTC)
1 3 5 7 9 11 13 15 17 19 21 23
0 -1 -2 -3 -4 -5 -6 -7 -8 -9
Flux (nmol m-2s-1)
May 2013
F
Fst

Figure

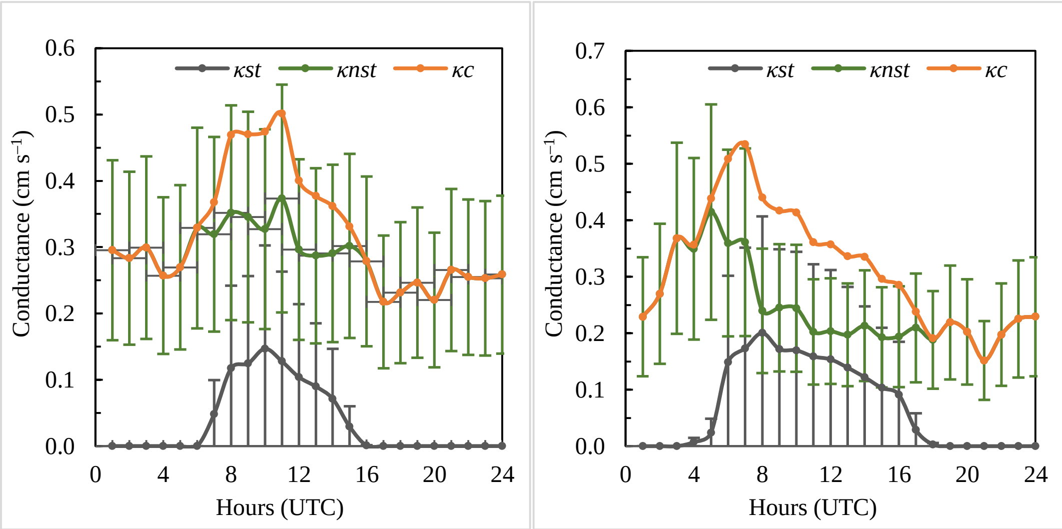
κst
κnst
κc
Conductance (cm s−1)
0.0
0.1
0.2
0.3
0.4
0.5
0.6
0.7
0
4
8
12
16
20
24
Hours (UTC)

Figure

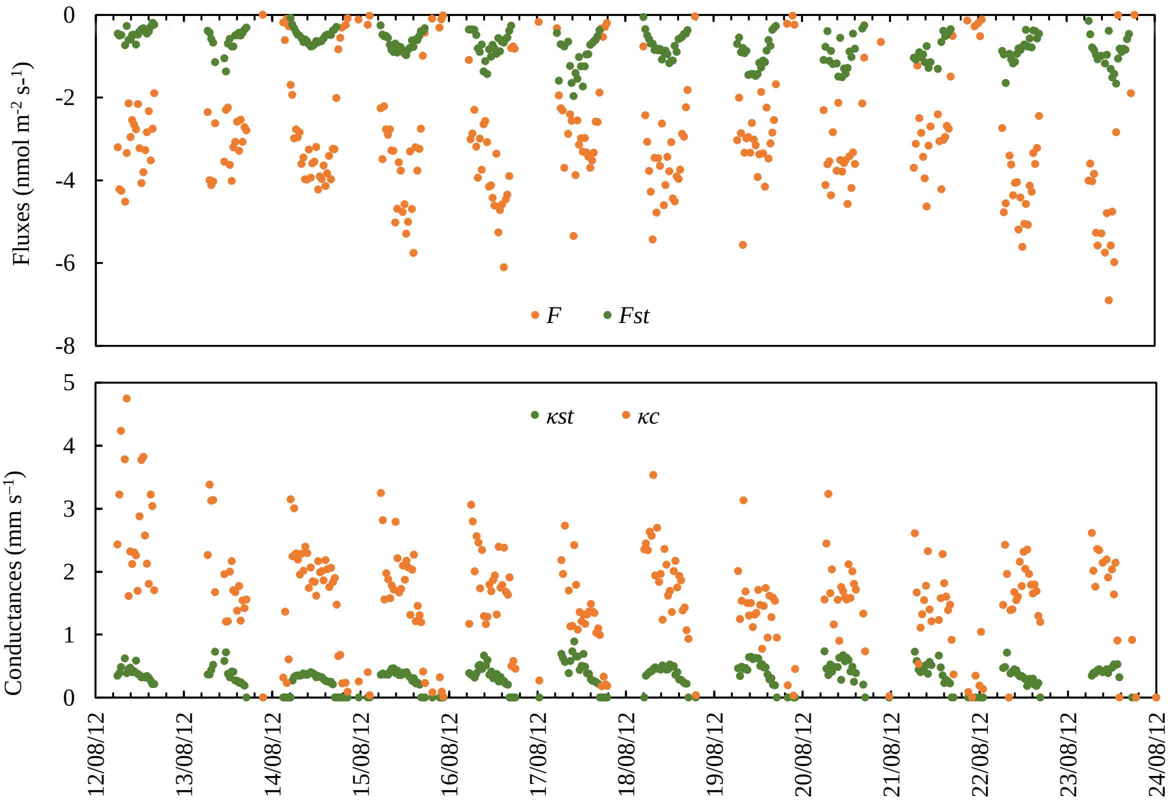
0
-2
-4
-6
-8
Fluxes (nmol m-2 s-1)
F
Fst
5
4
3
2
1
0
Conductances (mm s-1)
κst
κc
12/08/12
13/08/12
14/08/12
15/08/12
16/08/12
17/08/12
18/08/12
19/08/12
20/08/12
21/08/12
22/08/12
23/08/12
24/08/12

Figure

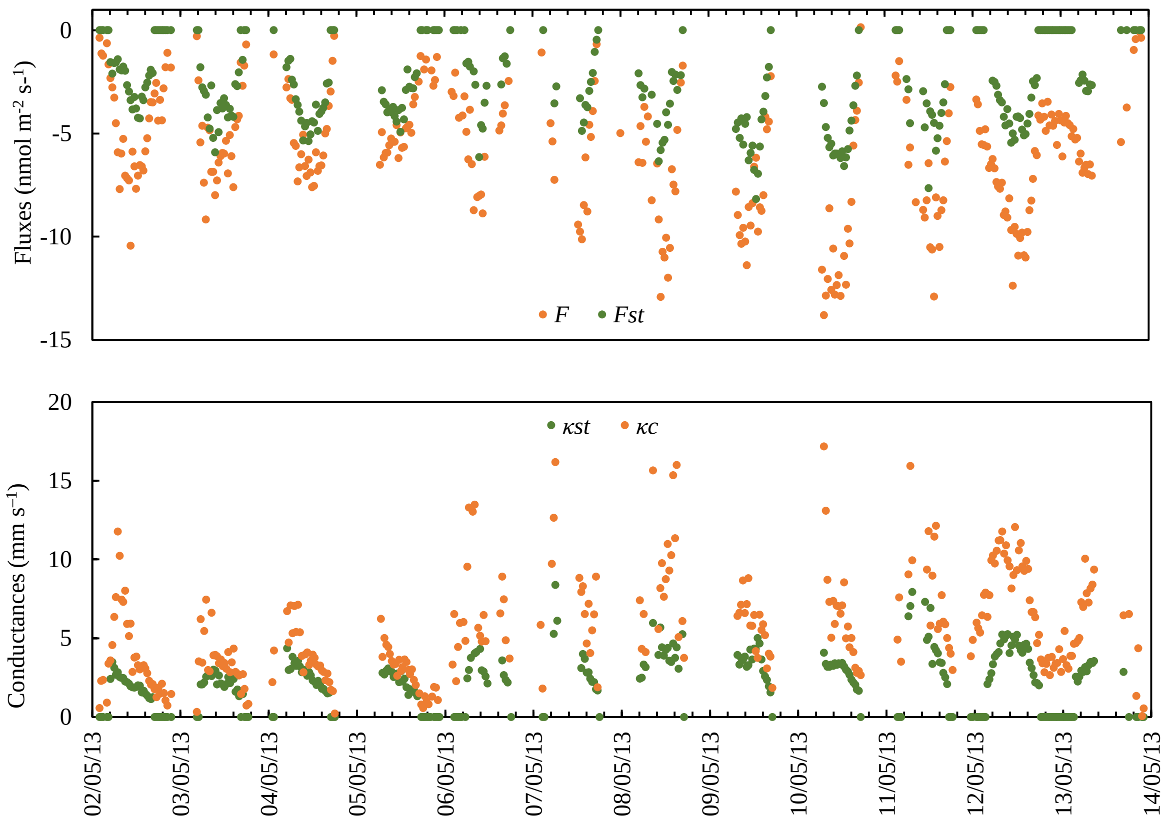
0
-5
-10
-15
Fluxes (nmol m-2 s-1)
F
Fst
20
15
10
5
0
Conductances (mm s-1)
κst
κc
02/05/13
03/05/13
04/05/13
05/05/13
06/05/13
07/05/13
08/05/13
09/05/13
10/05/13
11/05/13
12/05/13
13/05/13
14/05/13

table

Parameter	**Symbol**	**Instrument / method**	**Logging time**
sensible heat flux	H	CSAT3 ultrasonic anemometer / eddy covariance (EC)	0.1 s
latent heat flux	λE	CSAT3 ultrasonic anemometer + Li-Cor 7500 (EC)	0.1 s
momentum flux	τ	CSAT3 ultrasonic anemometer (EC)	0.1 s
net radiation	R_n	NR Lite net radiometer	30 min
ozone concentration (slow)	c	HORIBA APOA 350 ozone monitor	10 min
ozone concentration (fast)	c	ENVISCOPE fast response sensor	0.1 s
wind velocity	u	from CSAT3 ultrasonic anemometer	30 min
vegetation height	h	ruler at 5 × 40 cm^2 quadrats	1-2 weeks
above ground biomass	AGB	balance (samples from quadrats)	1-2 weeks
soil water content	θ	CS616 WC reflectometer at –0.03; –0.30 m	30 min
soil temperature	t_s	Campbell 105 T thermocouple at –0.05; –0.30 m	30 min
density of air	ρ	calculated from T, RH and p	30 min
relative humidity	RH	Väisälä HMP35AC	30 min
air temperature	t	Väisälä HMP35AC	30 min
air pressure	p	Li-Cor 7500	30 min
leaf area index	LAI	CEP-40 ceptometer (Decagon Devices, USA)	1-2 weeks
leaf surface wetness	LW	5 Bayreuth-type clips	30 min

Table 1 List of measurement methods.

table

Stability	No. of cases	TK3 corr. $\overline{w'c'}$	TK3 corr. $\overline{w'T'}$	Co-spectr. corr.	Semi-empir. corr. $\overline{w'c'}$
Unstable $-1 < \zeta \leq -0.1$	145	10.8±4.0%	3.6±1.3%	6.2±5.2%	10.0±5.4%
Near neutral $-0.1 < \zeta \leq 0.1$	317	16.9±4.3%	5.8±1.6%	7.1±5.5%	13.4±6.1%
Stable $0.1 < \zeta \leq 1$	127	18.8±6.2%	7.3±2.4%	5.6±5.0%	13.3±6.1%

note: TK3 corr. $\overline{w'c'}$ and TK3corr. $\overline{w'T'}$ are the TK3 spectral corrections for covariances (Mauder and Foken 2011); co-spectr. corr. are the maximum differences of relative co-spectrums for covariances (Ammann et al. 2006); semi-empirical corr. $\overline{w'c'}$: semi-empirical ozone flux correction (in %) calculated as: [(1+corr. $\overline{w'T'}$/100)×(1+Co-spectr. corr./100)–1]×100

Table 2 Mean value and relative error of different types of spectral corrections for ozone flux measurements in May 2013.

table

Season	Period	κ_{st} cm s^{-1}	κ_{nst} cm s^{-1}	κ_c cm s^{-1}	F nmol m^{-2} s^{-1}	F_{st} nmol m^{-2} s^{-1}
Vegetation	daytime	0.035±0.015	0.151±0.070	0.186±0.066	–3.33±1.17	–0.72±0.37
LAI = 0.25	night	0	= κ_c	0.032±0.031	–0.13±0.37	0
Vegetation	daytime	0.299±0.135	0.335±0.281	0.634±0.335	–6.87±2.69	–3.61±1.48
LAI = 1.04	night	0	= κ_c	0.311±0.193	–2.90±1.57	0
Winter	daytime	0	= κ_c	0.032±0.034	–0.42±0.42	0
snow	night	0	= κ_c	0.027±0.035	–0.31±0.33	0
Winter	daytime	0.008±0.005	0.467±0.228	0.475±0.227	–4.87±2.20	–0.104±0.052
no snow	night	0	= κ_c	0.233±0.216	–1.80±2.09	0

Table 3 Arithmetic mean and standard deviation (±1 σ) of stomatal (κ_{st}), non-stomatal (κ_{nst}) and canopy (κ_c) conductances, total flux (F) and stomatal flux (F_{st}) during daytime (R_g , $R > 0$ W m^{-2}) and night ($R_g = 0$ and $R < 0$ W m^{-2}).

Legends of figures

Fig 1 Comparison of water vapor flux calculated by Eq. (10) to eddy covariance measurements based on 14,688 half hourly measurements (2012 August – 2014 January). Dotted lines show the ±1 σ intervals.

Fig 2 Variation of the modelled stomatal conductance as a function of the main governing physical parameters (others are kept at constant values: R = 376 W m^{-2}; RH = 65%; LAI = 0.93).

Fig 3 Averaged daily ozone fluxes.

Fig 4 Diurnal variation of total (F) and stomatal (F_{st}) ozone flux in August 2012 with mean LAI = 0.25, (left); and in May 2013 with mean LAI = 1.05, (right).

Fig 5 Daily course of stomatal (κ_{st}), non-somatal (κ_{nst}), and canopy bulk (κ_c) conductances for the periods of the winter half-year (October-March), left; and the summer half-year (April-September), right. Each hourly average includes the previous two half-hour measurements. Note: during night $\kappa_c = \kappa_{nst}$. The error bars for κ_{st} and κ_{nst} are illustrated.

Fig 6 Variation of fluxes (top) and conductances of ozone (bottom) between 12-23 Aug. 2012 (LAI=0.19-0.31).

Fig 7 Variation of fluxes (top) and conductances of ozone (bottom) between 2-13 May 2013 (LAI=0.90-1.19).

Highlights

- evapotranspiration was partitioned into E_t and E_e parts by the SW model
- E_t was used to calculate stomatal conductance (κ_{st}) of ozone by the PM equation
- canopy conductance (κ_c) was calculated from eddy covariance measurement of O_3 flux
- stomatal and non-stomatal conductances were partitioned as $\kappa_c = \kappa_{st} + \kappa_{nst}$
- non-stomatal deposition of O_3 dominates especially for low *LAI* vegetation